The Genetic Diversity Mice Models in SARS-CoV-2 Infection

Xinpei Wang
Institute of Laboratory Animal Sciences
Yunpeng Liu
Institute of Laboratory Animal Sciences, CAMS & PUMC
Yajin Qu
Institute of Laboratory Animal Sciences, CAMS & PUMC
Rui Hou
Institute of Laboratory Animal Sciences, CAMS & PUMC
Jiangning Liu
Institute of Laboratory Animal Sciences, CAMS & PUMC
Ran Gao
Comparative Medicine Center, Peking Union Medical College (PUMC)
Linlin Bao
Peking Union Medical College
Wei Deng
Peking Union Medical College
Yunlong Cao
Peking University
Li Li
Institute of Laboratory Animal Sciences, CAMS & PUMC
Feifei Qi
Institute of Laboratory Animal Sciences, CAMS & PUMC
Qi Lv
Institute of Laboratory Animal Sciences, CAMS & PUMC
Fengli Li
Institute of Laboratory Animal Sciences, CAMS & PUMC
Xujian Liang
Institute of Laboratory Animal Sciences, CAMS & PUMC
Yu Cheng
Institute of Laboratory Animal Sciences, CAMS & PUMC
Lingyan Zhang
Institute of Laboratory Animal Sciences, CAMS & PUMC
Fan Ye
Institute of Laboratory Animal Sciences, CAMS & PUMC
Lanlan Lao
Institute of Laboratory Animal Sciences, CAMS & PUMC
Tianyu Lu
Institute of Laboratory Animal Sciences, CAMS & PUMC
Zhiqi Song
Institute of Laboratory Animal Sciences, CAMS & PUMC

Xuan Yu
Chinese Academy of Medical Sciences, Beijing https://orcid.org/0000-0001-6826-7260
Chuan Qin (qinchuan@pumc.edu.cn)
Institute of Laboratory Animal Sciences, CAMS & PUMC https://orcid.org/0000-0002-6261-1232

Article

Keywords: SARS-CoV-2, ACE2, genetic diversity, immune response, pathogenesis

Posted Date: April 27th, 2021

DOI: https://doi.org/10.21203/rs.3.rs-437876/v1

Abstract

The SARS-CoV-2 has led to a worldwide health crisis. The ACE2 has been identified as the entry receptor in a species-specific manner. Classic laboratory mice were insusceptible since the virus cannot use murine ACE2 orthologue. Animal models rely on gene modification on the virus or the host. However, these mice were restricted in limited genetic backgrounds and did not support natural infection. Here we showed two wild-type inbred lines (CAST and FEW) from Genetic Diversity mice supported authentic SARS-CoV-2 infection, and developed mild to moderate interstitial pneumonia, along with infiltrating inflammatory cells. Particularly, FEW featured age-dependent damages, while CAST charactered by pulmonary fibrosis. Genome and transcriptome comparative analysis suggested the mutated ACE2 was not responsible for SARS-CoV-2 infection in CAST and FEW, and the differential gene expressions in immune response and immune cell may be risk factors for the infection. In summary, the GD mice, derived from the multi-parental panel, provided promising murine models for exploring sophisticated pathogenesis in SARS-CoV-2.

Introduction

The pandemic of SARS-CoV-2 has infected more than 140 million people with over 3 million death and triggered a continuing global health emergency and economic crisis. The *ACE2* gene has been roundly demonstrated as the entry receptor for the SARS-CoV-2 in humans[1,2]. The infection of SARS-CoV-2 is initiated by the attachment of S protein to the *ACE2* receptor. Host cell protease, as *TMPRSS2* and *CatB/L*, facilitated the viral entry by cleaving S protein[1]. However, the recognition of coronavirus to its receptor was in a species-specific manner[3]. The *ACE2* ortholog in murine cannot effectively bind to SARS-CoV-2 S protein, as well as SARS-CoV-1, restraining viral entry in murine cell[4]. A variety of approaches were developed to overcome the interspecies barrier. h*ACE2*-expressing mice models were most used to elucidate the pathogenesis of SARS-CoV-2 (Table 1). h*ACE2* expression was controlled by various promoters (mouse *ACE2* promoter[2,5], *K18* promote[6], or *HFH4* promoter[7]), or delivered by ADV[8] and AAV-transfection[9]. Mouse-adaptive SARS-CoV-2 was also produced which was able to replicate in the airway of Balb/C mice[10,11]. While these mice models made tremendous contributions to explore the mechanism of viral infection, pathogenesis, and transmission, we also found the mice currently used were restricted to a few lines with single genetic background[12]. These most used classic laboratory inbred strains were generally derived from a few founder lines limited in the *M. m. Domesticus* subspecies[13,14]. As a result, the classic inbred lines were closely related to each other with limited genetic diversity and failed to reflect the complicated genetical polymorphism in humans[15,16]. There is an urgent need for naturally infected mice models with approved genetic diversity backgrounds and enabled authentic SARS-CoV-2 infection.

Table 1
Current mice model in SARS-CoV-2 infection

Murine Model	Genetic Background	*hAce2*	Inoculum	Phenotypes			Ref
				Lung pathology	Bodyweight loss	Outcomes	
K18 promoter	B6	**Y**	10^4 – 10^5 $TCID_{50}$ nCoV-WA1–2020	Severe	20–30%	Most died	6
Mouse *Ace2* promotor	ICR	**Y**	10^5 $TCID_{50}$ HB-01	Mild	8%	All recovered	2
Mouse *Ace2* promotor CRISPR/Cas9 knock-in		**Y**	$4×10^5$ PFU Wuhan/AMMS01/2020	Mild	10% (Aged only)	All recovered	5
HFH4 promoter	C3B6	**Y**	$7×10^5$ $TCID_{50}$ Wuhan/WIV04/2019	Severe (7 DPI)	5%	50 % survived	7
ADV transfection	Balb/C	**Y**	10^5 FFUs USA_WA1/2020	Serve (8 DPI)	10–25%	All recovered	8
AAV transfection	C57BL/6J	**Y**	10^6 PFU USA-WA1/2020	Mild	NS	No death	9
Balb/C	-	**N**	$1.6×10^4$ PFU Mice-adaptive virus	Age-related	Aged-only	No death	10,11
CAST/EiJ	Wild-derived	**N**	10^5 $TCID_{50}$ WH-09/human/2020/CHN	Pulmonary fibrosis	5%	90 % survived	This paper
FEW	Multi-genetic background	**N**	10^5 $TCID_{50}$ WH-09/human/2020/CHN	Age-related	20% (Aged only)	90 % survived	This paper

*Y indicated with hACE2 expression; N indicated without hACE2 expression; NS indicated no significant.

The Genetic Diversity Mice resources consisted of the inbred lines (also mentioned as Collaborative Cross, CC mice) and outbred stocks (also referred to as Diversity Outbred, DO mice) derived from the same multi-parental panel[17,18]. The founder lines contained five classic inbred strains and three wild-derived strains to maximize diversity, and represented

90% genetic variation across three subspecies, *M. m. musculus*, *M. m. domesticus*, and *M. m. castaneous*, making the GD mice possess genetic and phenotypic diversity on par with the human populations[15,16].

In this study, we assessed the susceptibility of SARS-CoV-2 across 23 Genetic Diversity inbred lines. Most strikingly, the line CAST and FEW could be naturally infected by patient-derived SARS-CoV-2, even without carrying the *hACE2* gene. Same as COVID-19 patients, the two susceptible lines supported viral replication and pathological changes in their lungs. We identified three humanized mutations in the *ACE2* sequence of FEW and CAST, which were then proved to making no sense in improving the affinity with SARS-CoV-2 RBD by *in vivo* and *in vitro* experiments. Transcriptome analysis indicated the differentially expressed genes involved in the immune barrier, immune response, and immune cell in FEW and CAST. Here we firstly reported the novel wild-type mice models that enable SARS-CoV-2 infection with the patient-derived virus, which also implied potentially more complicated host genetic factors for SARS-CoV-2 infection in addition to the essential host genes *ACE2*.

Results

Identification of the two SARS-CoV-2 susceptible lines from GD mice

Since murine *ACE2* does not support SARS-CoV-2 cellular entry, and *hACE2*-expressing mice models were produced to conquer the obstacles[5–9]. Here we used a total of 23 wild-type inbred lines from GD mice without hACE2 expression for SARS-CoV-2 infection (patient-derived virus). All the mice were intranasally infected at a dosage of 10^5 $TCID_{50}$ and monitored daily for weight loss, activity, response to external stimuli during the following five days (Fig. 1a). The results indicated 10/23 lines developed 5–15% weight loss, 10/23 strains showed less than 5% weight loss, while 3/23 lines exhibited slightly increased bodyweight after infection (Fig. 1b). Mice were sacrificed at 5 DPI, and major organs were collected for viral load detection and pathological observation. Interestingly, viral RNA was detectable in the lung tissues of CAST and FEW (Fig. 1c), implying the viral entry even in the absence of *hACE2* expression.

No death cases were declared among the twenty-one insusceptible lines, while one death case was reported respectively in FEW and CAST at 2 DPI (Fig. 1d). Moreover, compared to the young group of FEW, a significant weight loss was observed in the aged group (Fig. 1e), while little difference at the level of viral loads (Fig. 1f).

Pathological changes in GD mice as that of COVID-19 patients

Consistent with pathological findings in COVID-19 patients, we observed pathological damages in the two SARS-CoV-2 infected lines[19]. The viral RNA was visualized by ISH and viral protein was detected by IHC (Fig. 2a). In aged FEW, the virus was mainly detected in macrophages resident in bronchia and alveolar septum. Meanwhile, moderate interstitial pneumonia was developed in the aged FEW, characterized by thickened alveolar septa accompanied by infiltration of inflammatory cells in lung tissues. The bronchiolar epithelial cells showed swelling, some of which fragmented. The alveolar cavities were distended mainly by swollen macrophages, lymphocytes, and neutrophils. By comparison, only mild interstitial pneumonia developed in CAST and the young FEW, featured by fewer viruses in bronchial macrophages and very slightly thickened alveolar interstitium. Masson's staining suggested collagen fibers accumulated in the thickened alveolar interstitium in the lungs of CAST and FEW (aged group only). Other organs, including the brain, liver, kidney, duodenum, spleen, heart, testis, and epididymis were not affected (Fig. S1). Histopathological study for lines insusceptible to SARS-CoV-2, as YID and PWK were displayed in Fig. 2a and S2, and the mock group of FEW and CAST were shown in Fig. S3.

To investigate the infiltration of specific inflammatory cells, we performed the IHC assay to identify $MAC2^+$ macrophages, $CD3^+$ T lymphocytes, $CD4^+$ T lymphocytes, and $CD19^+$ B lymphocytes. As shown in Fig. 2b and S4, the majority type of infiltration of inflammatory cells in FEW and CAST was macrophages, then T lymphocytes.

ACE2 was not the primary cause for SARS-CoV-2 infection in GD mice

Coronavirus infection is initiated by cellular receptor recognition, and the interaction with viral receptors is the primary genetic determinant for host tropism[20,21]. SARS-CoV-2 utilizes the *ACE2* as the cell entry receptor in a species-specific way, that rendering most mice are insusceptible[22]. However, we identified two wild-type strains from the GD inbred mice that enabled SARS-CoV-2 infection. To explore the potential genetic mechanism, we compared the *ACE2* CDS sequences from the insusceptible and susceptible GD inbred lines with that of human and identified whether some key mutated residues facilitated viral entry in FEW and CAST.

Based on the *ACE2* sequence from the WGS data, three synonymous variants and four non-synonymous variants were identified in FEW and CAST (Fig. 3). The variants generated the following mutations in amino acid sequence: including three humanized mutations (in pink) glutamine (Q) to lysine (K) at site 309, alanine (A) to aspartic acid (D) at site 630, and threonine (T) to alanine (A) at site 774, and an additional mutation (in brown) from Valine (V) to isoleucine (I) at site 714. We also noticed the line of YID sharing completely the same *ACE2* sequence with FEW and CAST, but was verified to be SARS-CoV-2 insusceptible (Fig. 1C and 2A). Neither viral loads nor pathological changes were detected in YID in three independent experiments. The founder line PWK carried only one mutation at 309K (in Red), which also did not support SARS-CoV-2 infection (Fig. S2). Further, we examined the binding affinity of the humanized *ACE2* mutants to the SARS-CoV2-RBD-mFc protein. The humanized *ACE2* at 309K, 630D, and 774A did not show any increased affinity to the RBD domain (Fig. S5). Together the results indicated that despite the mutations in the *ACE2* CDS, they are not the majority reason for the SARS-CoV-2 infection in FEW and CAST.

Differential gene expression between the susceptible and insusceptible lines.

To further investigate the potential mechanism of SARS-CoV-2 infection in FEW and CAST, we performed the RNA sequence of lung tissues from both the susceptible and insusceptible lines. As shown in Fig. 4a, relative to the three insusceptible lines (YID, GIG, and FIM), there were 619 up-regulated and 863 down-regulated genes in FEW. Gene Ontology (GO) analysis of the down-regulated genes in FEW revealed the enrichment of gene clusters in immune response (including autoimmunity, adaptive immune response, chemokine receptors, cellular response to IFN-β and IFN-γ), immune cells (lymphocyte differentiation, T cell activation, and B cell proliferation) (Fig. 4c).

We next analyzed the differential gene expression across the five founder lines of GD mice. The transcriptome data was from the publication of Josset et al., (GSE52405)[23]. Comparing to the SARS-CoV-2 insusceptible lines (B6, 129, NOD, and PWK), we identified 351 up-regulated and 470 down-regulated genes in CAST (Fig. 4a). As shown in Fig. 4e, GO analysis of the down-regulated genes in CAST indicated enrichment of gene clusters in cilium organization and movement, and immune responses (PD-1 signaling, complement cascade regulation, T cell receptor signaling, cytokine productions)

To minimize the potential candidate genes involved in SARS-CoV-2 infection, we combined the results from {FEW *vs.* YID, FIM, GIG}, and {CAST *vs.* B6, 129S, NOD, PWK} (Fig. 4A). As a result, we identified a total of 18 up-regulated and 37 down-regulated genes in FEW and CAST (Fig. 4b). The heat map (Fig. 4d) was employed to display the differential gene expression in common between susceptible lines (FEW and CAST) and the insusceptible lines (FIM, GIG, YID, B6, NOD, 129, and PWK). As shown in Table 2, some of the genes have been verified as risk factors in SARS-CoV-2 infection. *HLA* played an essential role in the promotion of immune response to viral infection by presenting viral peptides at cell surface which were then recognized by cytotoxic cells. Down-regulation of *HLA-A* may be a risk factor for viral infection and immune evasion[24]. Several genes revolved in immune cell functions were down-regulated in FEW and CAST. *XCR1* was mainly expressed by DC cells which mediated immune response and promoted regulatory T cell development[25]. *CXCR3* which was expressed by T cells mediated the function of T cell and NK cell[26]. *CCL5* was expressed in T lymphocytes, macrophages, et al., which involved in leukocyte recruitment and NK cell activation[27]. *CD3E* was expressed at T cell membranes, and associated with T cell receptors, contributing to T cell development[28]. *SLPI* was secreted by epithelia,

and located at mucosal surfaces protecting the host via anti-pathogens and anti-inflammations[29]. *PON2*, as a lactonase with an anti-inflammatory effect, was down-regulated in FEW and CAST[30], while the *GSDMA* (expressed by epithelial cells and contributed to the pyrotosis pathway) was up-regulated[31]. The above indicated that several risk factors in SARS-CoV-2 infection were abnormally expressed in FEW and CAST. Further study will focus on whether these risk factors co-operated or separated for SARS-CoV-2 infection in FEW and CAST.

Table 2
Differential expressed genes participated in SARS-CoV-2 in FEW and CAST

GENE		Expression	Potential Role in SARS-CoV	Ref
H2-Q4	Down	Human ortholog *HLA-A*, expressed by a variety of cell types, belonged to the HLA class I heavy chain paralogues.	*HLA-A* played essential role in viral antigen presentation pathway. Host genetic variations in *HLA-A* were associated with susceptibility to SARS-CoV-2 infection or the severity of COVID-19	66,67
XCR1	Down	A *GPCR* protein, expressed by a DC subpopulation, participated in DC-mediated immune response and development of regulatory T cells.	The gene cluster at locus 3p21.31, including *SLC6A20*, *LZTFL1*, *CCR9*, *FYCO1*, *CXCR6* and *XCR1*, was identified as a susceptibility locus in patients with COVID-19 with respiratory failure	25,42,68
CXCR3	Down	Primarily expressed by CD4 + and CD8 + T cells, which binds *CXCL9*, *CXCL10*, and *CXCL11*.	The reduced expression of *CXCL9*, *CXCLI10*, *CXCL11*, and their receptor *CXCR3* in aged COVID-19 patients, resulted in deficiencies in tracking and/or function of cytotoxic T and NK cells.	26,43
CCL5	Down	Ubiquitously expressed by T lymphocytes, macrophages, platelets, et al, involved in leukocytes recruiting, and activating of particular NK cells to generate chemokine-activated killer cells.	The high level of innate immune cytokines and chemokines, associated with severe COVID-19. Male patients had higher plasma levels of innate immune cytokines and chemokines including IL-8, IL-18, and CCL5, accounting for the sex biases in COVID-19.	27,44,69
SLPI	Down	A non-glycosylated low molecular protein expressed at mucosal surfaces and secreted by epithelial cells, with high affinity for the neutrophil serine proteinases, elastase and cathepsin G.	*SLPI* protects the host via anti-bacterial, fungal, viral, inflammatory, and anti-proteolytic. The increased *SLPI* in SARS-CoV infected lung suggesting the onset of the inflammatory process.	29,41,70
CD3E	Down	*CD3-epsilon* forms heterodimers as T-Cell receptor-CD3 complex, functioned in T-cell development, defects in CD3E resulted in immunodeficiency.	The *CD4, CD3E, FGL2, LCK* and *SELL* are associated with activation and binding of T lymphocytes associated with poor outcome in COVID-19.	45
PON2	Down	A lactonase displayed anti-oxidant and anti-inflammatory properties. PON2 deficiency results in vascular inflammation and abnormalities in blood coagulation.	Mendelian randomization analysis identified *IFNAR2*, *TRIM5*, *NLRC5*, *MCTP1*, *PTPN1*, *FCER1G*, *ATF4* and *PON2* involved in cytokine storm and venous thromboembolism in COVID-19.	30,46
GSDMA3	Up	GSDMA expressed in epithelia cells are pore-forming proteins participate in the immune response.	GSDMs are critical components of pyroptosis pathways induced by inflammasome activation. Presence or absence of GSDMs is important for clinical symptoms of COVID-19	40

Discussion

Accompanied by the global pandemic of SARS-CoV2, there is a pressing demand for uncovering the sophisticated relationship between viral infection and host genetic. As is well-known, the host genes *ACE2* and *TMPRSS2* are essential for viral infection, and the recognition between SARS-CoV-2 and its cellular receptor is species-specific[1,20,21] Accordingly, wild-type mice failed to be infected by SARS-CoV-2 due to the limited affinity of murine *ACE2* to SARS-CoV-2 RBD[22]. Therefore, mice models in SARS-CoV-2 infection relied on genetic modification on the host or the virus. *hACE2*-expressing mice model and mouse-adapted viruses were extensively applied in investigating viral entry, transmission, pathogenesis, therapies, and vaccine evaluations[2,5–9]

In this study, we screened the susceptibility of SARS-CoV-2 across 23 GD inbred strains by using the patient-derived virus. Surprisingly, the line CAST and FEW allowed SARS-CoV-2 infections, and developed mild to moderate interstitial pneumonia after infection, along with infiltrating macrophages, lymphocytes, and neutrophils, in conformity to the COVID-19 patients[19]. Simultaneously, we also observed some differences between FEW and CAST after the infection. Age-dependent damages were induced by SARS-CoV-2 in FEW. The aged group (13-month-old) was characterized by significant bodyweight loss, moderate interstitial pneumonia, and pulmonary fibrosis. By contrast, the young group (4-month-old) exhibited slightly decreased bodyweight and mild interstitial pneumonia without notable thickened alveolar interstitium nor pulmonary fibrosis. Since COVID-19 patients in older age were associated with severer clinical manifestations and longer disease courses, we identified FEW as a promising mouse model to illuminate the age-related risk factors in COVID-19[32–34]. In CAST, as one of the founder lines of GD mice, only mild interstitial pneumonia was observed after infection, but pulmonary fibrosis was induced even at a young age. Pulmonary fibrosis accounted for chronic breathing difficulties and long-term disability, bringing negative impacts on the life quality of COVID-19 patients[35,36]. The specific mechanism for pulmonary fibrosis in COVID-19 patients was still unclear, and we identified a potential mouse model for future study on the genetic basis of pulmonary fibrosis, also for the evaluation of potential therapeutic strategies.

Genome and transcriptome sequencing were employed to explore the potential mechanism of SARS-CoV-2 infection in GD mice. Comparative analysis of the *ACE2* sequence revealed three humanized mutations in FEW and CAST. However, the YID, carrying an identical *ACE2* sequence with FEW and CAST, was insusceptible to SARS-CoV-2. Meanwhile, the humanized mutated *ACE2* showed no increased affinity to SARS-CoV-2 RBD *in vitro*. Differentially expressed genes in lung tissues were analyzed between the susceptible and non-susceptible lines, implying the differential gene expression in lung tissues of FEW and CAST. The differentially expressed genes, particularly for these down-regulated genes, revealed the enrichment of gene clusters probably contributing to SARS-CoV-2 susceptibility in FEW and CAST. To be specific, the cilia regulations represented physiological and immune barriers possessing a positive effect on viral clearance was down-regulated in FEW and CAST[37]. Genes participating in anti-viral immune responses were also down-regulated, including regulation of chemokines and cytokines, cellular response to IFNs and complement system, as well as modulations of innate/adaptive immune cells (NK cells, T cells, B cells) [38,39]. Potential candidate genes, related to viral-host interaction (*HLA-A*[40] and *SLPI*[41]), immune cellular responses (*XCR1*[42], *CXCR3*[43], *CCL55*[44], *CD3E*[45]), and inflammations (*PON2*[46] and *GSMDA3*[40]) were risk factors already documented in SARS-CoV-2 infections. Altogether, we speculated the *ACE2* may not be responsible for SARS-CoV-2 infection in FEW and CAST, and a potentially novel mechanism involved in the initiation of SARS-CoV-2 infection in the two wild-type strains.

In summary, we investigated the susceptibility of SARS-CoV-2 among GD inbred strains and identified two lines as new mice models for SARS-CoV-2 infection. The Genetic Diversity mice, derived from the most used laboratory inbred (B6, A/J, NOD, NZO, 129S), and three wild-derived inbred (WSB, CAST, and PWK), were demonstrated to be powerful tools for the research on complex trait due to their diversity in both genotype and phenotype[17,18]. Before this, the GD mice already used in a variety of infectious diseases, as Ebola (mice-adapted)[47], Influenza[48], and SARS-CoV (mice-adapted)[49,50], providing

new insight into the relationship between the virus and host genetic. Here we presented evidence for infection of patient-derived SARS-CoV-2 in the GD inbred mice without *hACE2* expression. The FEW exhibited an age-related pathological change as the aged population in COVID-19 patients, while the CAST was featured by pulmonary fibrosis after infection. Lessons from the GD mice implied the knowledge of host genes for SARS-CoV-2 may not be limited to a few genes. Future studies in GD mice may also rely on Recombinant inbred cross (RIX) between the two GD inbred lines. Hybridization of SARS-CoV-2 susceptible lines to the others lines which are typical of immunocompromised, obese, diabetic, malignant, may elicit more phenotypes to underline the comorbidities in COVID-19 patients.

Methods

Ethics statement

All procedures were performed in the Animal Biosafety Level 3 (ABSL3) facility with HEPA-filtered isolators. All studies involving animals were evaluated and approved by the Institutional Animal Care and Use Committee of the Institute of Laboratory Animal Sciences (ILAS), Peking Union Medical College, Approval ID: QC20003.

Viruses and cells

The SARS-CoV-2 isolated by ILAS, assigned as SARS-CoV-2/WH-09/human/2020/CHN. Vero cells, maintained as the previous description, were used for the reproduction of SARS-CoV-2 stock[51]. Virus titer of the supernatant was determined using a standard 50% tissue culture infection dose ($TCID_{50}$) assay.

Mice

A total of 23 GD inbred lines were used in this study, including 18 lines from ILAS and 5 founder lines purchased from the Jackson Laboratory (CAST/EiJ 000735, 129S1/SvlmJ 002448, NOD/ShiLtJ 001976, PWK/PhJ 003715, A/J 000646). The Special-Pathogen-Free (SPF) animals were housed and bred in temperature- and humidity-controlled facility, kept on a 12/12 light/dark cycle, and provided with standardized rodent chow and drinkable water.

Infection Procedures

Adult mice were euthanized by intraperitoneal injection with 2.5% avertin at 0.02 mL/g. The SARS-CoV-2 stock virus at a dosage of 10^5 $TCID_{50}$ inoculated intranasally by using a pipette. All mice were monitored daily to record bodyweight changes, activities, response to external stimuli. The infected mice were sacrificed and dissected at 5 DPI, tissue samples were collected for virus load detection and histopathological study.

Viral RNA analysis

The lungs were homogenized by an electric homogenizer. After centrifuged at 3,000 rpm (10 min, 4°C), the supernatants were collected for RNA extraction. Total RNA was extracted with the RNeasy Mini Kit (Qiagen, Germany), and reverse transcription was performed by using the PrimerScript RT Reagent Kit (TaKaRa, Japan). A quantitative real-time reverse transcription-PCR (qRT-PCR) reaction was performed as previous study[2]. Primer sequences targeted in the envelope (E) gene of SARS-CoV-2 as followed: Sense: 5’- TCGTTTCGGAAGAGACAGGT-3’, Anti-sense 5’-GCGCAGTAAGGATGGCTAGT-3’.

Pathological analysis

Major organs, including lungs, livers, hearts, spleens, kidneys, brains, and small intestines were fixed in 10% formalin solution, and paraffin sections (3–4 μm in thickness) were processed routinely. Hematoxylin and Eosin (HE) stain and modified Masson's Trichrome stain were used to identify histopathological changes. All the slides were blinded reviewed by pathologists from ILAS Pathology Laboratory.

Immunohistochemistry (IHC)

Paraffin-embedded slides were placed in 1x Antigen Retrieval Buffer, and antigen retrieval was processed by heating the slides in microwave for high power (3 min), medium (5 min), and low power (3 min) respectively. Then cool down the slides to room temperature,and blocking in 1% normal goat serum for 20 min. The slides were incubated with primary antibodies in 4 ℃ overnight, including SARS-CoV-2 Spike S1 antibody (GeneTex, GTX635654, 1:500), MAC2 antibody (Cedarlane Laboratories, CL8942AP,1:1000), CD3 antibody (Abcam, ab11089,1:500); CD4 (Abcam, ab183685, 1:1000); CD19 antibody (Abcam, ab245235,1:1000). The Goat anti-rat IgG secondary antibody (HRP) (Beijing ZSGB Biotechnology, PV9004), or Goat anti-rabbit IgG secondary antibody (HRP) (Beijing ZSGB Biotechnology, PV9001) were added and incubated at 37 ℃ for 60 min. After incubating with 3,30-diaminobenzidine tetrahydrochloride (DAB), the slices were counterstained with hematoxylin, dehydrated, and mounted on a slide. All slides were blinded reviewed for identified the virus and immune cell infiltration.

In situ Hybridization (ISH)

To examine SARS-CoV-2 genomic RNA in FFPE tissues, ISH was applied by the RNAscope® 2.5 HD Reagent Kit-RED (Advanced Cell Diagnostic, ACD, Cat No. 322310) as previous description[52]. Briefly, ISH Probe-V-nCoV2019-S (positive-sense RNA probe, Cat No. 848561, ACD) (Genomic RNA fragment 21631–23303, RefSeq #NC_045512.2) was prepared. Tissue sections were deparaffinized by xylene, washed by ethanol washes and blocked by peroxidase, and then were heated in an antigen retrieval buffer and digested in the proteinase. After that, sections were incubated with target probe at 40°C in a hybridization oven for 2 h. After rinsing, ISH signal was amplified by the pre-amplifier and amplifier conjugated to alkaline phosphatase, and then incubated with DAB for visualization. Then, the sections were stained with hematoxylin, air-dried, mounted, and stored for observation and analysis.

Genome sequence analysis

Genome DNA was extracted from tail tissue by using DNeasy Blood & Tissue Kit (Cat# 69504, Qiagen), and sequenced by BGI (China). The raw data were processed by removing reads 1) containing sequencing adapter; 2) whose low-quality base ratio is more than 50%; 3) whose 'N' base ratio is more than 10%. The clean data were then aligned to the mouse reference genome GRCm38.p5 using Burrows-Wheeler Aligner (BWA)[53]. Picard was employed to remove duplicated sequence reads (Picard Toolkit 2019, Broad Institute, GitHub Repository; http://broadinstitute.github.io/picard/). Realignment was performed with the Genome Analysis Toolkit (GATK)[54]. Finally, alignment result files (in BAM format) were prepared for downstream analysis. Bazam (version 1.0.1) was used to extract the CDS sequence of *ACE2* from BAM files[55]. The extracted reads were realigned on GRCm38.p5 coordinates using BWA and exported into BAM files. These BAM files were then sorted and indexed as the prerequisite input BAM file for SAMtools mpileup function (version 0.1.19)[56]. Finally, *ACE2* CDS sequences were called with SAMtools mpileup and for each position of the coding region, reads alignments form a vertical slice covering the whole region. All vertical slices from the 23 inbred strains were merged into one table.

RNA-Seq

Total RNA was isolated from lung tissues by using RNeasy Mini Kit (Qiagen, Germany) according to the manufacturer's protocol. Total RNA was qualified and quantified with Agilent 2100 bioanalyzer. A minimum RNA integrity value of 7.0 was required for library preparation and sequencing. mRNA was purified by Oligo(dT)-attached magnetic beads, and fragmented into small pieces. First-strand cDNA was generated using random hexamer-primed reverse transcription, followed by second-strand cDNA synthesis. The cDNA fragments obtained from the previous step were amplified by PCR after end repair, and the products were purified by Ampure XP Beads and validated by Agilent 2100 bioanalyzer for quality control. Afterwards, the double-stranded PCR products were heated denatured and circularized by the splint oligo sequence. The single-strand circle DNA (ssCir DNA) was formatted as the final library which was further amplified with phi29 to make DNA nanoball (DNB) containing more than 300 copies per molecular. DNBs were loaded into the patterned nanoarray and single end 50 bases reads were generated on BGIseq500 platform (BGI, China). The sequencing data were

filtered with SOAPnuke (v1.5.2)[57] by removing reads 1) containing sequencing adapter; 2) whose low-quality base ratio is more than 20%; 3) whose 'N' base ratio is more than 5%. The clean reads were stored in FASTQ format and mapped to the mouse reference genome GRCm38.p6 using HISAT2 (v2.0.4)[58]. Bowtie2 (v2.2.5)[59] was applied to align the clean reads to the reference coding gene set, and the expression levels of genes were calculated by RSEM (v1.2.12)[60].

Transcriptome data analysis

Josset et al. performed RNA-seq on lung tissues from the 8 founder lines of cc mice, the raw RNA-seq data of the mock group were obtained from NCBI Gene Expression Omnibus (GEO, GSE52405) [23]. Differential gene expression profiles were obtained across the founder lines used in current research, including A/J, B6, 129, NOD, PWK, CAST.

Differential gene expression analyses of lung tissues among the ten inbred lines were performed by using the R package DESeq2 (v1.30.0)[61] and edgeR (v3.32.0)[62,63]. Genes with an adjusted P-value (Benjamini-Hochberg Procedure) < 0.05 and fold change (log2) > 1 were considered significant. Common differentially expressed genes in CAST and FEW strains were filtered and processed in downstream analysis. Venn diagrams were generated via http://bioinformatics.psb.ugent.be/webtools/Venn/. Pathway and biological process enrichment analyses of differentially expressed genes were performed using Metascape[64], and the results were visualized by Seaborn (https://seaborn.pydata.org).

ACE2/RBD binding assay:

RBD proteins purchased from Sino Biological Inc (Cat# 40592-V05H). Binding assay was performed as previous described[65]. Briefly, ELISA plates were coated with RBD or ACE2 (mutated) protein at 4°C overnight. After standard blocking and washing, his-tagged ACE2 (mutated) or BRD protein was added. After 2 h of incubation at room temperature (RT), plates were washed and anti-his/HRP was added. After 1 h incubation at RT, the chromogen solution was used as the substrate, and absorbance at 450 nm was measured by a microplate reader.

Statistical analysis

All statistical analysis were analyzed by Student's t-test and two-way ANOVA with GraphPad Prism 8.0 (GraphPad Software, San Diego, CA, USA). A p value < 0.05 was considered statistically significant.

Abbreviations

129: 129S1/SvlmJ

AAV: Adenovirus Associated Virus

ACE2: Angiotensin- converting enzyme 2

ADV: Adenovirus

ARDS: Acute respiratory distress syndrome

C57BL/6J: B6

CAST/EiJ: CAST

CatB/L: Endosomal cysteine proteases cathepsin B and L

CC mice: Collaborative Cross mice

CCL5: chemokine (C-C motif) ligand 5

CD3E: CD3 antigen, epsilon polypeptide

CDS: Coding sequence

COVID-19: Coronavirus disease 2019

CXCR3: Chemokine (C-X-C motif) receptor 3

DC: Dendritic cell

DPI: Days post-infection

DO mice: Diversity outbred mice

FFUs: Focus-forming units

Genetic Diversity mice: GD mice

GPCRs: G protein coupled receptors

GSDMs: Gasdermins

HLA: human leukocyte antigen

HFH4: Hepatocyte forkhead homologue 4

ISH: *In-situ* hybridization

IHC: Immunohistochemistry

NOD: NOD/ShiLtJ

PD-1: Programmed death-1

PON2: Paraoxonase 2

PWK: PWK/PhJ

RBD: Receptor-binding domain

SARS: Severe acute respiratory syndrome

SLPI: Secretory leukocyte peptidase inhibitor

Spike protein: S protein

TMPRSS2: Type 2 transmembrane serine protease

WGS: Whole genome sequence

XCR1: X-C Motif Chemokine Receptor

Declarations

Competing interests

The authors declare no conflicts of interest.

Author Contribution

C.Q. conceptualized the project and reviewed the manuscript; Methodology: X.W., J.L., R.H., and R.G.; Investigation: X.W., R.H., Y.L., Y.Q., L.B., W.D., Y.C., L.L., F.Q., Q.L., F.L., X.L., Y.C., L.Z., F.Y., L.L., X.Y.; Writing-draft: X.W., Writing-editing: C.Q., R.G., J.L., T.L., Z.S.; Funding Acquisition: C.Q.; Resources: C.Q.; Supervision: C.Q.

Acknowledgement

The sincere thanks to Prof. Grant Morahan (University of Western Australia) and Fuad A. Iraqi (Tel Aviv University) for their efforts on the development of the Genetic Diversity Mice. This work was supported by the National Natural Science Foundation of China (82041008), Bill & Melinda Gates Foundation (INV-006371), the 111 Project (B20095), the Fundamental Research Funds for the Central Universities, CAMS (2019-RC-HL-011).

References

1. Hoffmann, M. *et al.* SARS-CoV-2 Cell Entry Depends on ACE2 and TMPRSS2 and Is Blocked by a Clinically Proven Protease Inhibitor. *Cell* (2020). doi:10.1016/j.cell.2020.02.052
2. Bao, L. *et al.* The pathogenicity of SARS-CoV-2 in hACE2 transgenic mice. *Nature* (2020). doi:10.1038/s41586-020-2312-y
3. Li, F. Receptor recognition mechanisms of coronaviruses: a decade of structural studies. *J. Virol.* **89**, 1954–1964 (2015).
4. Shang, J. *et al.* Structural basis of receptor recognition by SARS-CoV-2. *Nature* (2020). doi:10.1038/s41586-020-2179-y
5. Sun, S. H. *et al.* A Mouse Model of SARS-CoV-2 Infection and Pathogenesis. *Cell Host Microbe* (2020). doi:10.1016/j.chom.2020.05.020
6. Yinda, C. K. *et al.* K18-hACE2 mice develop respiratory disease resembling severe COVID-19. *PLoS Pathog.* (2021). doi:10.1371/journal.ppat.1009195
7. Jiang, R. Di *et al.* Pathogenesis of SARS-CoV-2 in Transgenic Mice Expressing Human Angiotensin-Converting Enzyme 2. *Cell* (2020). doi:10.1016/j.cell.2020.05.027
8. Hassan, A. O. *et al.* A SARS-CoV-2 Infection Model in Mice Demonstrates Protection by Neutralizing Antibodies. *Cell* **182**, 744-753.e4 (2020).
9. Israelow, B. *et al.* Mouse model of SARS-CoV-2 reveals inflammatory role of type i interferon signaling. *J. Exp. Med.* (2020). doi:10.1084/JEM.20201241
10. Dinnon, K. H. *et al.* A mouse-adapted model of SARS-CoV-2 to test COVID-19 countermeasures. *Nature* (2020). doi:10.1038/s41586-020-2708-8
11. Gu, H. *et al.* Adaptation of SARS-CoV-2 in BALB/c mice for testing vaccine efficacy. *Science (80-.).* (2020). doi:10.1126/science.abc4730
12. Singh, A. *et al.* A Comprehensive Review of Animal Models for Coronaviruses: SARS-CoV-2, SARS-CoV, and MERS-CoV. *Virologica Sinica* (2020). doi:10.1007/s12250-020-00252-z
13. Justice, M. J. & Dhillon, P. Using the mouse to model human disease: increasing validity and reproducibility. *Dis. Model. Mech.* **9**, 101–103 (2016).
14. Roberts, A., Pardo-Manuel de Villena, F., Wang, W., McMillan, L. & Threadgill, D. W. The polymorphism architecture of mouse genetic resources elucidated using genome-wide resequencing data: implications for QTL discovery and systems genetics. *Mamm. Genome* **18**, 473–481 (2007).

15. Beck, J. A. *et al.* Genealogies of mouse inbred strains. *Nature Genetics* (2000). doi:10.1038/71641
16. Wade, C. M. *et al.* The mosaic structure of variation in the laboratory mouse genome. *Nature* (2002). doi:10.1038/nature01252
17. Threadgill, D. W., Miller, D. R., Churchill, G. A. & de Villena, F. P. M. The collaborative cross: A recombinant inbred mouse population for the systems genetic era. *ILAR J.* (2011). doi:10.1093/ilar.52.1.24
18. Churchill, G. A., Gatti, D. M., Munger, S. C. & Svenson, K. L. The Diversity Outbred mouse population. *Mamm. Genome* (2012). doi:10.1007/s00335-012-9414-2
19. Polak, S. B., Van Gool, I. C., Cohen, D., von der Thüsen, J. H. & van Paassen, J. A systematic review of pathological findings in COVID-19: a pathophysiological timeline and possible mechanisms of disease progression. *Mod. Pathol.* **33**, 2128–2138 (2020).
20. Li, R., Qiao, S. & Zhang, G. Analysis of angiotensin-converting enzyme 2 (ACE2) from different species sheds some light on cross-species receptor usage of a novel coronavirus 2019-nCoV. *J. Infect.* **80**, 469–496 (2020).
21. Douam, F. *et al.* Genetic Dissection of the Host Tropism of Human-Tropic Pathogens. *Annu. Rev. Genet.* **49**, 21–45 (2015).
22. Liu, Y. *et al.* Functional and genetic analysis of viral receptor ACE2 orthologs reveals a broad potential host range of SARS-CoV-2. *Proc. Natl. Acad. Sci. U. S. A.* **118**, e2025373118 (2021).
23. Josset, L. *et al.* Annotation of long non-coding RNAs expressed in collaborative cross founder mice in response to respiratory virus infection reveals a new class of interferon-stimulated transcripts. *RNA Biol.* **11**, 875–890 (2014).
24. Shkurnikov, M. *et al.* Association of HLA Class I Genotypes With Severity of Coronavirus Disease-19. *Front. Immunol.* **12**, 641900 (2021).
25. Lei, Y. & Takahama, Y. XCL1 and XCR1 in the immune system. *Microbes Infect.* **14**, 262–267 (2012).
26. Karin, N. CXCR3 Ligands in Cancer and Autoimmunity, Chemoattraction of Effector T Cells, and Beyond. *Front. Immunol.* **11**, 976 (2020).
27. Aldinucci, D. & Colombatti, A. The inflammatory chemokine CCL5 and cancer progression. *Mediators Inflamm.* **2014**, 292376 (2014).
28. Fischer, A., de Saint Basile, G. & Le Deist, F. CD3 deficiencies. *Curr. Opin. Allergy Clin. Immunol.* **5**, (2005).
29. Majchrzak-Gorecka, M., Majewski, P., Grygier, B., Murzyn, K. & Cichy, J. Secretory leukocyte protease inhibitor (SLPI), a multifunctional protein in the host defense response. *Cytokine Growth Factor Rev.* **28**, 79–93 (2016).
30. Costa, L. G. *et al.* Paraoxonase-2 (PON2) in brain and its potential role in neuroprotection. *Neurotoxicology* **43**, 3–9 (2014).
31. Orning, P., Lien, E. & Fitzgerald, K. A. Gasdermins and their role in immunity and inflammation. *J. Exp. Med.* **216**, 2453–2465 (2019).
32. Liu, Y. *et al.* Association between age and clinical characteristics and outcomes of COVID-19. *Eur. Respir. J.* **55**, 2001112 (2020).
33. Wu, C. *et al.* Risk Factors Associated With Acute Respiratory Distress Syndrome and Death in Patients With Coronavirus Disease 2019 Pneumonia in Wuhan, China. *JAMA Intern. Med.* **180**, 934–943 (2020).
34. Takagi, H. Risk and protective factors of SARS-CoV-2 infection. *J. Med. Virol.* **93**, 649–651 (2021).
35. Lechowicz, K. *et al.* COVID-19: The Potential Treatment of Pulmonary Fibrosis Associated with SARS-CoV-2 Infection. *J. Clin. Med.* **9**, 1917 (2020).
36. George, P. M., Wells, A. U. & Jenkins, R. G. Pulmonary fibrosis and COVID-19: the potential role for antifibrotic therapy. *Lancet. Respir. Med.* **8**, 807–815 (2020).
37. Nunnari, G. *et al.* Network perturbation analysis in human bronchial epithelial cells following SARS-CoV2 infection. *Exp. Cell Res.* **395**, 112204 (2020).

38. Schön, M. P. *et al.* COVID-19 and immunological regulations - from basic and translational aspects to clinical implications. *J. Dtsch. Dermatol. Ges.* **18**, 795–807 (2020).
39. Kulkarni-Munje, A. *et al.* Disease-duration based comparison of subsets of immune cells in SARS CoV-2 infected patients presenting with mild or severe symptoms identifies prognostic markers for severity. *Immunity, Inflamm. Dis.* 10.1002/iid3.402 (2021). doi:10.1002/iid3.402
40. Cui, H. & Zhang, L. Key Components of Inflammasome and Pyroptosis Pathways Are Deficient in Canines and Felines, Possibly Affecting Their Response to SARS-CoV-2 Infection. *Front. Immunol.* **11**, 592622 (2021).
41. Kong, S. L., Chui, P., Lim, B. & Salto-Tellez, M. Elucidating the molecular physiopathology of acute respiratory distress syndrome in severe acute respiratory syndrome patients. *Virus Res.* **145**, 260–269 (2009).
42. Group, S. C.-19 G. *et al.* Genomewide Association Study of Severe Covid-19 with Respiratory Failure. *N. Engl. J. Med.* **383**, 1522–1534 (2020).
43. Lieberman, N. A. P. *et al.* In vivo antiviral host transcriptional response to SARS-CoV-2 by viral load, sex, and age. *PLoS Biol.* **18**, e3000849–e3000849 (2020).
44. Shaath, H., Vishnubalaji, R., Elkord, E. & Alajez, N. M. Single-Cell Transcriptome Analysis Highlights a Role for Neutrophils and Inflammatory Macrophages in the Pathogenesis of Severe COVID-19. *Cells* **9**, 2374 (2020).
45. Parkinson, N. *et al.* Dynamic data-driven meta-analysis for prioritisation of host genes implicated in COVID-19. *Sci. Rep.* **10**, 22303 (2020).
46. Liu, D. *et al.* Mendelian randomization analysis identified genes pleiotropically associated with the risk and prognosis of COVID-19. *J. Infect.* **82**, 126–132 (2021).
47. Rasmussen, A. L. *et al.* Host genetic diversity enables Ebola hemorrhagic fever pathogenesis and resistance. *Science (80-.).* (2014). doi:10.1126/science.1259595
48. Leist, S. R. *et al.* Influenza H3N2 infection of the collaborative cross founder strains reveals highly divergent host responses and identifies a unique phenotype in CAST/EiJ mice. *BMC Genomics* (2016). doi:10.1186/s12864-016-2483-y
49. Gralinski, L. E. *et al.* Genome Wide Identification of SARS-CoV Susceptibility Loci Using the Collaborative Cross. *PLoS Genet.* (2015). doi:10.1371/journal.pgen.1005504
50. Graham, J. B. *et al.* Baseline T cell immune phenotypes predict virologic and disease control upon SARS-CoV infection in Collaborative Cross mice. *PLoS Pathog.* **17**, e1009287–e1009287 (2021).
51. Bao, L. *et al.* Transmission of SARS-CoV-2 via close contact and respiratory droplets among hACE2 mice. *J. Infect. Dis.* (2020).
52. Song, Z. *et al.* SARS-CoV-2 Causes a Systemically Multiple Organs Damages and Dissemination in Hamsters. *Front. Microbiol.* **11**, 618891 (2021).
53. Li, H. & Durbin, R. Fast and accurate short read alignment with Burrows-Wheeler transform. *Bioinformatics* **25**, 1754–1760 (2009).
54. McKenna, A. *et al.* The Genome Analysis Toolkit: a MapReduce framework for analyzing next-generation DNA sequencing data. *Genome Res.* **20**, 1297–1303 (2010).
55. Sadedin, S. P. & Oshlack, A. Bazam: a rapid method for read extraction and realignment of high-throughput sequencing data. *Genome Biol.* **20**, 78 (2019).
56. Li, H. *et al.* The Sequence Alignment/Map format and SAMtools. *Bioinformatics* **25**, 2078–2079 (2009).
57. Li, R., Li, Y., Kristiansen, K. & Wang, J. SOAP: short oligonucleotide alignment program. *Bioinformatics* **24**, 713–714 (2008).
58. Kim, D., Langmead, B. & Salzberg, S. L. HISAT: a fast spliced aligner with low memory requirements. *Nat. Methods* **12**, 357–360 (2015).

59. Langmead, B. & Salzberg, S. L. Fast gapped-read alignment with Bowtie 2. *Nat. Methods* **9**, 357–359 (2012).
60. Li, B. & Dewey, C. N. RSEM: accurate transcript quantification from RNA-Seq data with or without a reference genome. *BMC Bioinformatics* **12**, 323 (2011).
61. Love, M. I., Huber, W. & Anders, S. Moderated estimation of fold change and dispersion for RNA-seq data with DESeq2. *Genome Biol.* **15**, 550 (2014).
62. Robinson, M. D., McCarthy, D. J. & Smyth, G. K. edgeR: a Bioconductor package for differential expression analysis of digital gene expression data. *Bioinformatics* **26**, 139–140 (2010).
63. McCarthy, D. J., Chen, Y. & Smyth, G. K. Differential expression analysis of multifactor RNA-Seq experiments with respect to biological variation. *Nucleic Acids Res.* **40**, 4288–4297 (2012).
64. Zhou, Y. *et al.* Metascape provides a biologist-oriented resource for the analysis of systems-level datasets. *Nat. Commun.* **10**, 1523 (2019).
65. Cao, Y. *et al.* Potent Neutralizing Antibodies against SARS-CoV-2 Identified by High-Throughput Single-Cell Sequencing of Convalescent Patients' B Cells. *Cell* **182**, 73-84.e16 (2020).
66. Habel, J. R. *et al.* Suboptimal SARS-CoV-2-specific CD8(+) T cell response associated with the prominent HLA-A*02:01 phenotype. *Proc. Natl. Acad. Sci. U. S. A.* **117**, 24384–24391 (2020).
67. Nguyen, A. *et al.* Human Leukocyte Antigen Susceptibility Map for Severe Acute Respiratory Syndrome Coronavirus 2. *J. Virol.* **94**, e00510-20 (2020).
68. Lee, J.-W., Lee, I.-H., Sato, T., Kong, S. W. & Iimura, T. Genetic variation analyses indicate conserved SARS-CoV-2-host interaction and varied genetic adaptation in immune response factors in modern human evolution. *Dev. Growth Differ.* 10.1111/dgd.12717 (2021). doi:10.1111/dgd.12717
69. Takahashi, T. *et al.* Sex differences in immune responses that underlie COVID-19 disease outcomes. *Nature* **588**, 315–320 (2020).
70. Williams, S. E., Brown, T. I., Roghanian, A. & Sallenave, J.-M. SLPI and elafin: one glove, many fingers. *Clin. Sci.* **110**, 21–35 (2005).

Figures

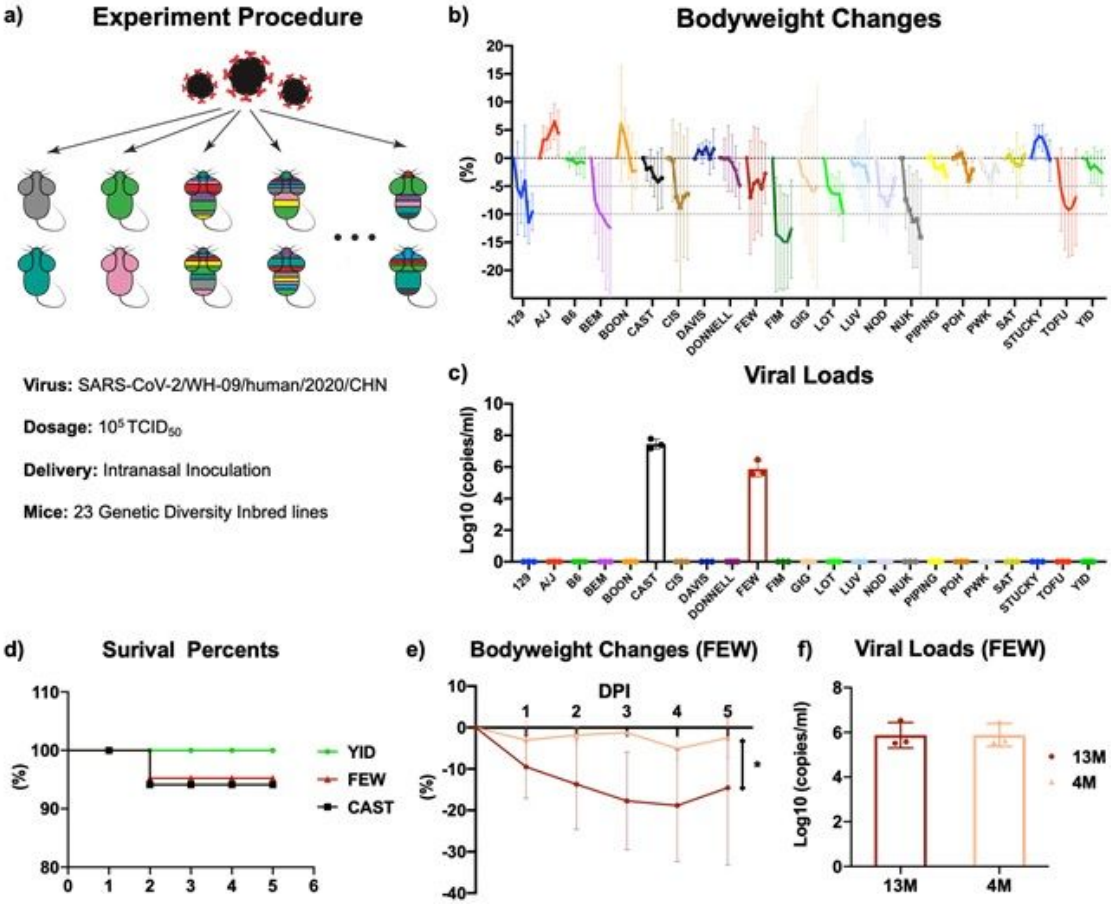

Figure 1

Identification of SARS-CoV-2 susceptible lines from GD mice a) Schematic of experiment procedure. Adult mice from 23 GD inbred lines were infected with SARS-CoV-2 by intranasal inoculation. All mice were monitored daily and sacrificed at 5 DPI. Tissue samples were collected for analysis. b) Bodyweight changes in the 23 GD lines were recorded from 0 to 5 DPI, n=3. c) Viral RNA from lung homogenates was measured by qPCR against SARS-CoV-2 at 5 DPI, n=3. d) Survival percent among the SARs-CoV-2 YID (insusceptible) and FEW & CAST (susceptible). e) A significant decline in bodyweight in the aged FEW (13-month-old) than that in the young group (4-month-old) from 0 to 5 DPI, p=0.0376. f) No difference in viral load between the 4M and 13M FEW at 5 DPI.

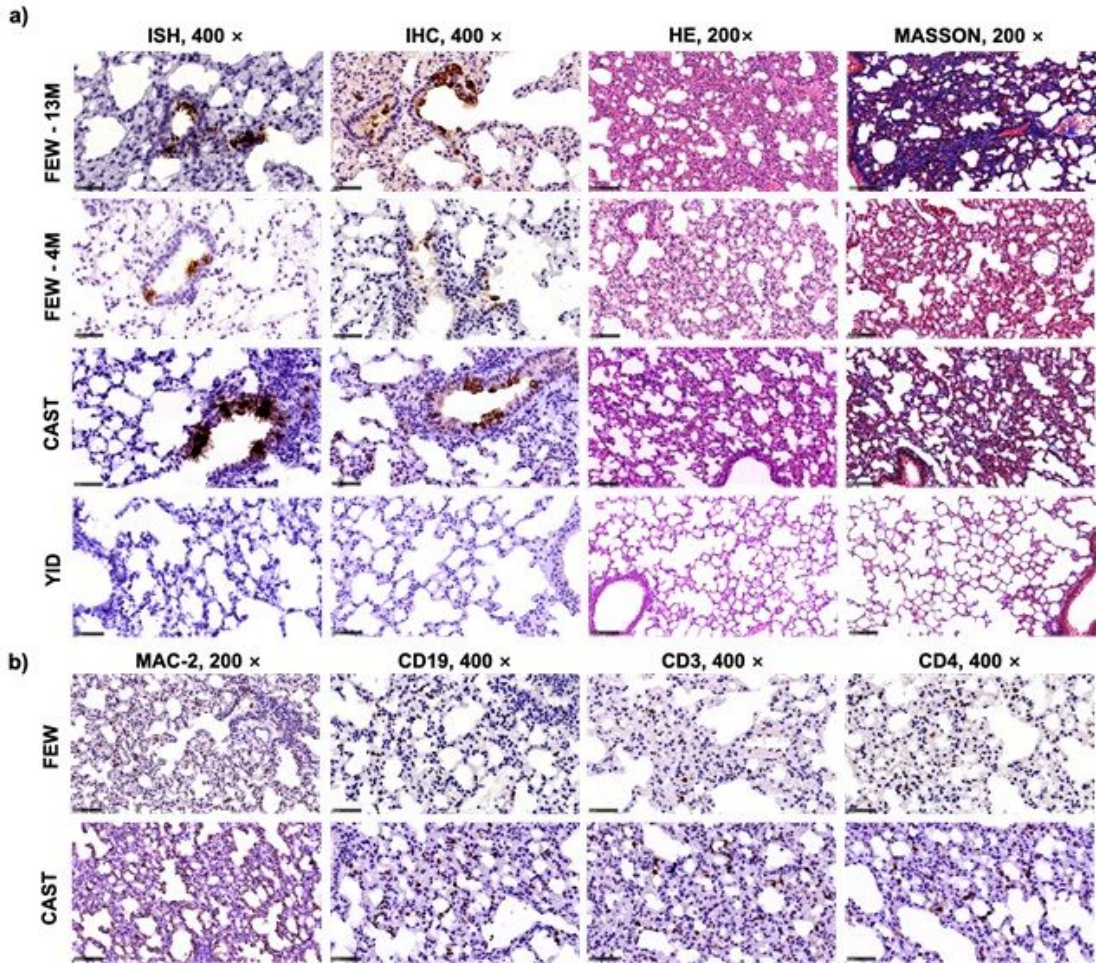

Figure 2

Pathological studies in susceptible (FEW/CAST) and insusceptible (YID) lines. a) Viral RNA was detected by ISH and viral S protein was detected by IHC in FEW (4 M and 13 M), CAST, and YID. Histopathological changes in lungs were observed by HE staining, and collagenous fibers were observed by Masson staining. b) IHC was carried out to investigate the infiltration of inflammatory cells in SARS-CoV-2 infected FEW and CAST, including MAC2+ macrophages, CD19+ B lymphocytes, CD3+ and CD4+ T lymphocytes.

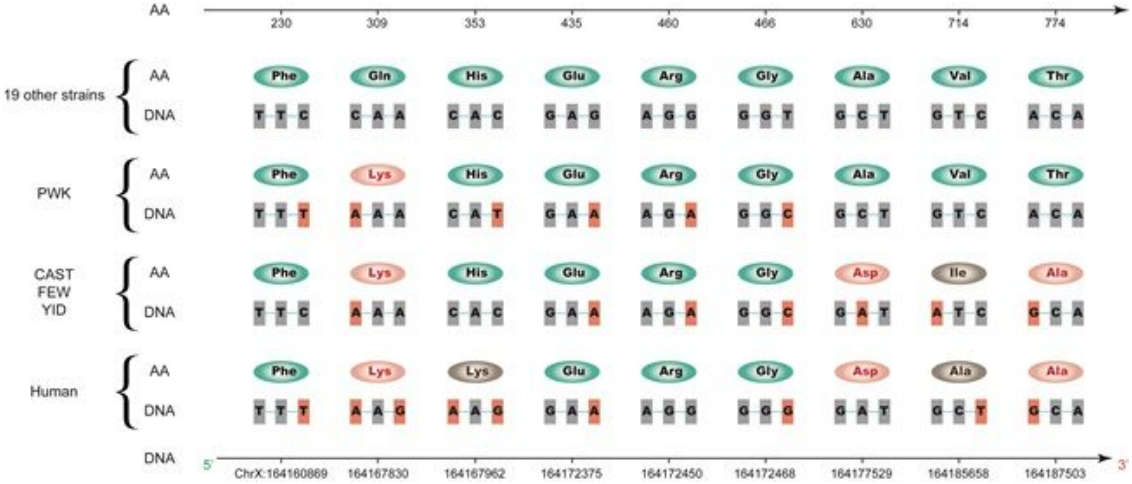

Figure 3

Screening of ACE2 CDS sequence among GD inbred lines and human Alignment of the ACE2 sequences, including the amino acid sequence and CDS DNA sequence. Four synonymous and three non-synonymous variants were identified in ACE2 CDS among the 23 GD strains. Comparing with the human ACE2, FEW, CAST, and YID possessed three humanized mutations at 309K, 630D, and 774A (in Red), as well as an extra mutation at 774I (in Brown) in amino acid sequence. The founder line PWK possessed only one mutation at 309K (in Red), while no mutations were identified in the left of 19 GD strains.

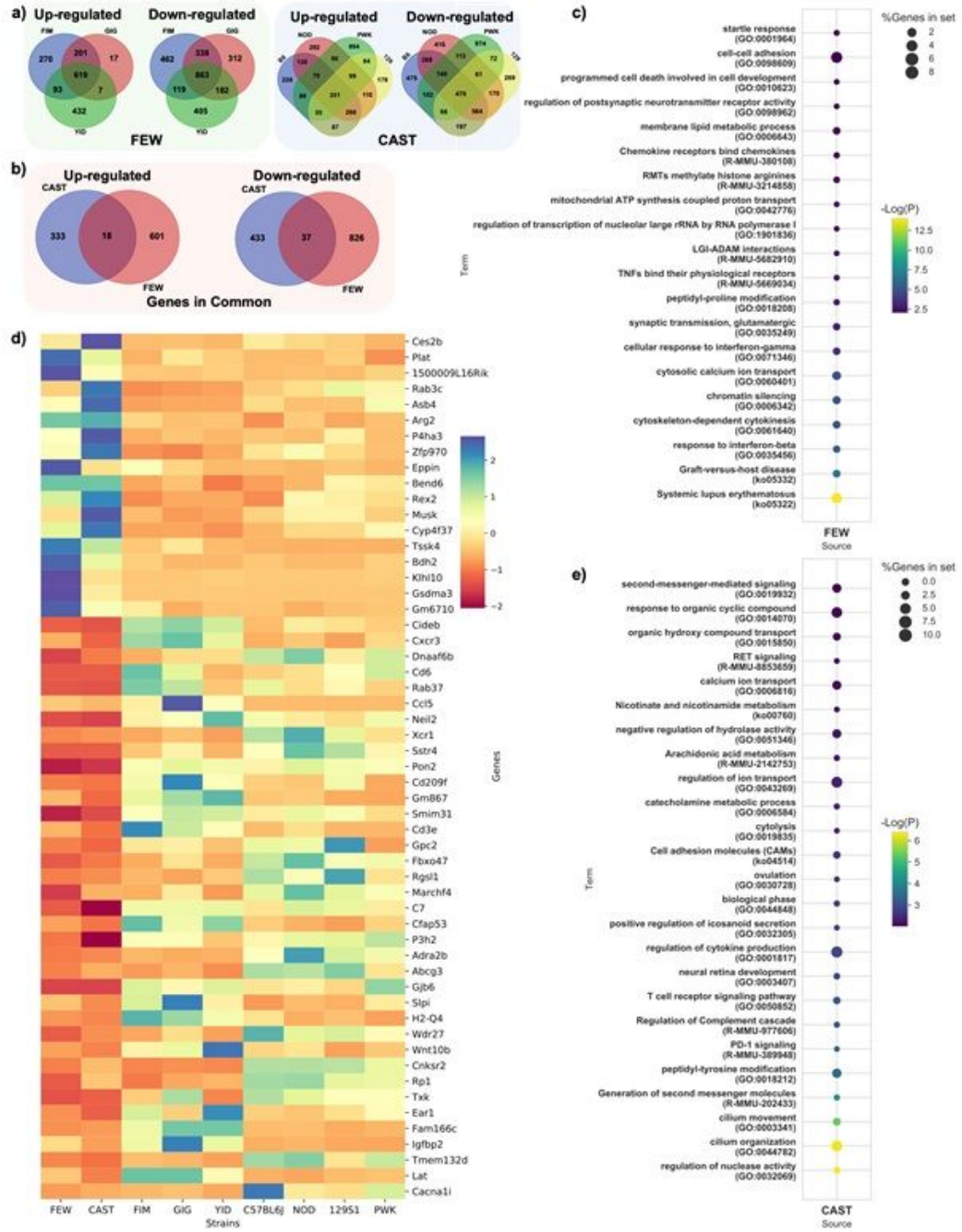

Figure 4

Transcriptome differences analysis between the susceptible and insusceptible lines a) Differential gene expression in FEW vs. YID, FIM, and GIG (Green panel), CAST vs. B6, 129, NOD, and PWK (Blue panel). b) 18 up-regulated and 37 down-regulated common genes in FEW and CAST. c) Heat map was graphed for differentially expressed genes of FEW and CAST in common. d) Dotplot visualization of GO enrichment was performed for significantly down-regulated genes in FEW by using STRING against the GO dataset. e) Dotplot of GO enrichment for significantly down-regulated genes in

CAST. The color of the dots represents -log(p) for each enriched GO term, and the size represents the percentage of genes enriched.

Supplementary Files

This is a list of supplementary files associated with this preprint. Click to download.

- Supplementary.pdf